Available online at www.sciencedirect.com

ScienceDirect

Energy Procedia 63 (2014) 693 – 702

Energy Procedia

GHGT-12

Evaluation of microporous biochars produced by single-step oxidation for postcombustion CO_2 capture under humid conditions

M.G. Plaza, A.S. González, F. Rubiera, C. Pevida*

Instituto Nacional del Carbón, INCAR-CSIC, Apartado 73, 33080 Oviedo, Spain

Abstract

Water vapor is the third component of flue gases after N_2 and CO_2. The permanent dipole moment of the water molecule makes it strongly adsorbable on many adsorbents, which can negatively affect the adsorption capacity of carbon dioxide (even causing an irreversible loss in certain cases). Carbon materials have high stability in moist conditions and present a hydrophobic nature that makes these materials appealing adsorbents for post-combustion CO_2 capture. Furthermore, these adsorbents present the added advantage that can be obtained from a globally available, cheap and renewable source of carbon: biomass. In the present work the effect of water vapor on the adsorption performance of CO_2 using a microporous biochar developed from olive stones by single-step oxidation is evaluated. The equilibrium of adsorption of water vapor on the selected biochar was studied in a wide temperature range that is considered of interest for the post-combustion case (12.5-85 °C). This biochar presents a moderate water adsorption capacity and type V adsorption isotherms, which will facilitate the desorption of water vapor during cyclic operation. Breakthrough curves were obtained using a gas mixture which composition resembled flue gas in the presence and absence of water vapor. The breakthrough curves of CO_2 obtained under dry and humid conditions overlap each other, which indicates that the presence of water vapor does not hinder CO_2 adsorption in the short time scale. Moreover, the adsorbent recovered its full adsorption capacity after regeneration. These findings point out that this material could be used to separate CO_2 from humid flue gas using cyclic adsorption processes.

Peer-review under responsibility of the Organizing Committee of GHGT-12

Keywords: CO_2 capture; adsorption; water vapor; carbon

* Corresponding author. Tel.: +34-985-119-090; fax: +34-985-297-662.
E-mail address: cpevida@incar.csic.es

Peer-review under responsibility of the Organizing Committee of GHGT-12
doi:10.1016/j.egypro.2014.11.077

1. Introduction

The main component of flue gases is N_2 (> 65 %), followed by lower amounts of CO_2, H_2O and O_2. Trace amounts of NO_x and SO_x can be found after the purification units, although these are not expected to interfere significantly in a physisorption process. In general, CO_2 is preferentially adsorbed over the major flue gas component, N_2, due to its stronger quadrupole moment. Many adsorption studies evaluate the potential of CO_2 adsorbents solely in terms of their adsorption capacity in pure CO_2 or, in best cases, by their CO_2/N_2 selectivity. However, a significant amount of water vapor is also present in flue gases. For example, the gas stream leaving a wet scrubber in a coal fired power plant will be nearly saturated with water vapor. Even in the cases where no desulfurization unit is needed, flue gases will contain water vapor coming from the fuel and the combustion air. Moreover, the permanent dipole moment of water molecules makes them strongly adsorbed by many adsorbents, which difficults the adsorbent regeneration. Therefore, water adsorption can cause a drastic decrease in the adsorption capacity to carbon dioxide, which can even be irreversible in certain cases. For this reason, adsorption separation units sometimes include a dehumidification stage with alumina to avoid co-adsorption of water vapor by zeolites [1]. The use of hydrophobic adsorbents, such as carbon materials, can eliminate the need of such step entailing additional installation and operating costs. Thus, it is of utmost interest to evaluate the effect of water vapor on the CO_2 capture performance of candidate adsorbents.

Biomass is a globally available and renewable source of carbon. Carbon adsorbents with a low carbon footprint can be easily obtained from agricultural residues or food industry by-products, through relatively simple heat treatment processes. The gases and tars released during the process can be burned *in situ* to reduce the energy requirements of the process, or collected for bio-oil or chemicals production. The solid fraction, sometimes referred to as *biochar*, is a low-cost and microporous carbon that presents selectivity towards CO_2 and high stability in moist environments. These properties make this material an appealing adsorbent for postcombustion CO_2 capture applications.

In this work, a microporous biochar produced by single-step oxidation of olive stones is evaluated as CO_2 adsorbent in postcombustion conditions. The use of air as the activating gas provides cost savings due to the cheaper cost of the gas feedstock, and to the lower activation temperatures required, compared to conventional activation with H_2O or CO_2. In a previous work [2], the effect of activating conditions on the CO_2 adsorption capacity of the biochars was evaluated. It was observed that the use of rarefied air (3 % O_2, balance N_2) at moderate temperatures (650 °C) lead to microporous carbons with a very narrow microporosity (0.3-0.5 nm), useful for CO_2 adsorption at low partial pressures, which is the case of postcombustion applications (3-33 % CO_2 at near atmospheric pressure [3]). Here the focus is placed on the effect of water vapor on the adsorption performance of CO_2. First, the equilibrium of adsorption of water vapor on the selected biochar was studied in a wide temperature range which is considered of interest for the post-combustion case (12.5-85 °C), and compared to that of CO_2 and N_2. Secondly, the breakthrough curves of a binary N_2/CO_2 mixture which composition resembled dry flue gas were obtained and compared to the breakthrough curves of a ternary $N_2/CO_2/H_2O$ mixture which composition resembled humid flue gas.

Nomenclature

α_μ	critical water cluster size to enter the micropores
ε	total void fraction of the fixed-bed
C_{calc}	amount adsorbed calculated using the adsorption model
C_{exp}	amount of H_2O adsorbed measured with the static volumetric apparatus
C_i	amount of species *i* adsorbed at a given time calculated from the breakthrough experiments
C_{DJD}	amount of H_2O adsorbed calculated by the DJD model
$C_{\mu s}$	saturation capacity for the adsorption of water on the micropores
$F_{i,in}$	molar flow rate of species *i* fed to the adsorber
$F_{i,out}$	molar flow rate of species *i* in the effluent
k_f	chemisorption equilibrium constant
k_μ	micropore equilibrium constant

$k_{R\mu}$	relaxation equilibrium constant for water desorption from the micropores
m	maximum number of water molecules that could form around one single functional group
N	number of experimental data points considered
P	absolute pressure
p^0	saturation pressure
pH_{PZC}	point of zero charge
S_0	oxygen functional group concentration on the carbon surface
R	Universal constant of gases
RH	Relative humidity (%)
T	temperature
x	relative pressure *(x = p/p0)*
y_i	molar fraction of species i in the gas mixture
V_b	fixed-bed volume
V_d	dead volume of the adsorber
w	mass of adsorbent loaded in the adsorber column

2. Materials and methods

2.1. Adsorbent properties

The adsorbent used in this work, was obtained by single-step activation with rarefied air (3 % O_2, balance N_2) at moderate temperatures (650 °C) departing from a biomass residue: olive stones. Sample preparation and characterization details can be found elsewhere [2]. Table 1 summarizes the most relevant physicochemical properties of the adsorbent.

Table 1. Adsorbent characteristics

Solid density[a] (kg m^{-3})		1684
Particle density[b] (kg m^{-3})		759
Bed density [c](kg m^{-3})		421
Elemental analysis (wt.% daf)	C	95.0
	H	1.7
	N	0.0
	S	0.0
	O	3.3
Ash content (wt.% db)		3.9
pH_{PZC}		10.3

[a] Determined by helium pycnometry; [b] Determined by mercury intrusion at 0.1 MPa; [c] Determined experimentally in the fixed-bed adsorber; daf: dry ash free basis; db: dry basis.

2.2. Equilibrium of adsorption of pure components

The equilibrium of adsorption of CO_2 and N_2 in the temperature range between 0 and 50 °C of the olive stone biochar was assessed in a previous study [2]. The adsorption isotherms of H_2O over OS were obtained in a volumetric apparatus Hydrosorb 1000 from Quantachrome Instruments at different temperatures: 12.5, 25, 50, 70 and 85 °C up to the corresponding saturation pressure.

2.3. Fixed-bed experiments

Breakthrough experiments were carried out using synthetic flue gas mixtures in the presence and absence of water vapor to evaluate its effect on CO_2 adsorption. These experiments were carried out in a fixed-bed adsorption unit described in detail elsewhere [4]. The adsorber consists on a stainless steel column with 9.12 mm of internal diameter carefully packed with 3.8 g of adsorbent. The "dry" synthetic flue gas is prepared by mixing individual streams of CO_2 and N_2 which flow is set by means of mass flow controllers. In the wet experiments, the N_2 stream is humidified prior to be mixed with the dry CO_2 stream. The relative humidity of the gas mixture is monitored continuously by a humidity probe located in the effluent line. To make sure that the feed composition was stable, this was analyzed before starting the experiment bypassing the adsorber. At t = 0 the feed was redirected to the adsorber, which was initially full of helium at 25 °C and 150 kPa. The effluent flow rate is measured by means of a mass flow meter located between the humidity probe and a dryer column that removes the water vapor prior to analyze the CO_2 and N_2 content of the effluent using a gas micro-chromatograph. The "dry" and "wet" breakthrough experiments were repeated to confirm the results obtained, regenerating the bed with helium flow at 150 °C between consecutive runs. The experimental conditions are summarized in Table 2 in chronological order.

Table 2. Fixed bed experiments

	T (°C)	P (kPa)	Feed flow rate [a] (g/h)	RH[a] (%)	y_{CO2}[a]
Run 1 ("dry")	25	150	14.6	2	0.15
Run 2 ("wet")	25	150	14.7	65	0.15
Run 3 ("dry")	25	150	14.7	3	0.15
Run 4 ("wet")	25	150	14.7	65	0.15

[a] At t = 0

3. Results and discussion

3.1. Equilibrium of adsorption of water vapor

The water vapor adsorption isotherms are shown in Figure 1a in terms of amount adsorbed *versus* absolute pressure. At a given partial pressure of water vapor the amount adsorbed decreases with increasing temperature due to the shift of the saturation pressure. In fact, when the amount adsorbed is represented *versus* the partial pressure (Figure 1b), the isotherms at the different temperatures virtually overlapped.

The water vapor adsorption isotherms present a Type V topology with a small uptake at low relative pressures and a narrow hysteresis loop, which is indicative of the narrow microporosity of the evaluated biochar [2, 5]. Note that the adsorption is reversible: water vapor can be desorbed at constant temperature by simply lowering its partial pressure. This equilibrium behavior would facilitate the regeneration in a VSA process, reducing considerably the pumping cost compared to polar adsorbents like zeolites and alumina that present adsorption isotherms of Type I and II, respectively, with high uptakes from low relative pressures.

The isosteric heat of adsorption of water vapor on the evaluated biochar, which is a measure of the strength of adsorption, was calculated from the slope of the experimental isosteres using the Clausius-Clapeyron relation (correlation coefficients above 0.99). It presents an average value of 44 kJ mol^{-1} which is close to the heat of condensation of water in the temperature range evaluated [6], as expected for a physisorption process. On the other hand, Zeolite 13 X, presents a stronger adsorption of water vapor, with a value of the isosteric heat of adsorption between 54 and 62 kJ mol^{-1} [7], which would increase the energy required to regenerate the adsorbent.

It is important to highlight that the saturation capacity of water vapor on the evaluated biochar is relatively low compared to other carbon adsorbents [4, 8, 9]. For example, this adsorbent presents nearly one third of the maximum adsorption capacity of an activated carbon derived from the same precursor by direct activation with CO_2 [4]. This is mainly attributed to the lower texture development attained by activation with rarefied air compared to the activation with CO_2 [2, 4, 10]. In fact, the initial upswing of the adsorption isotherms at relative pressures below 0.1 are alike,

which suggests that the slight differences in the surface chemistry of these carbons are not the cause of the different water vapor adsorption behavior. The lower equilibrium capacity even at high relative pressures is also an important advantage from the point of view of the final application, as this will reduce the amount of water vapor coadsorbed with CO_2 from the humid flue gases. In a VSA process, for example, this would reduce the pumping energy required to regenerate the adsorbent [8].

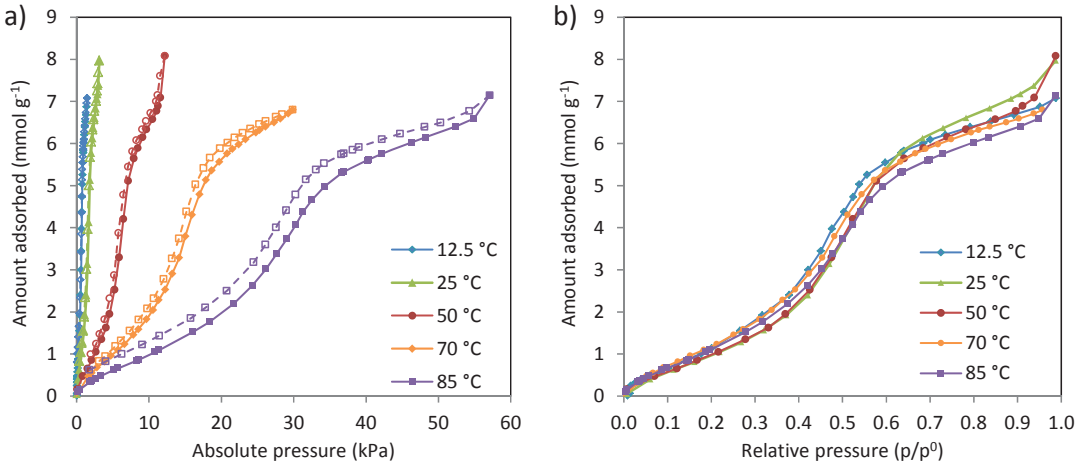

Fig. 1. Water vapor adsorption isotherms: (a) amount adsorbed *vs.* absolute pressure; (b) amount adsorbed *vs.* relative pressure. Filled symbols and solid lines represent the adsorption branch and empty symbols and dashed lines the desorption branch.

Despite the hydrophobic nature of carbons, the adsorption capacity of water vapor at high relative pressures (*ie*, high relative humidity) is still higher than that of CO_2 at the same temperature (see Figure 2a).

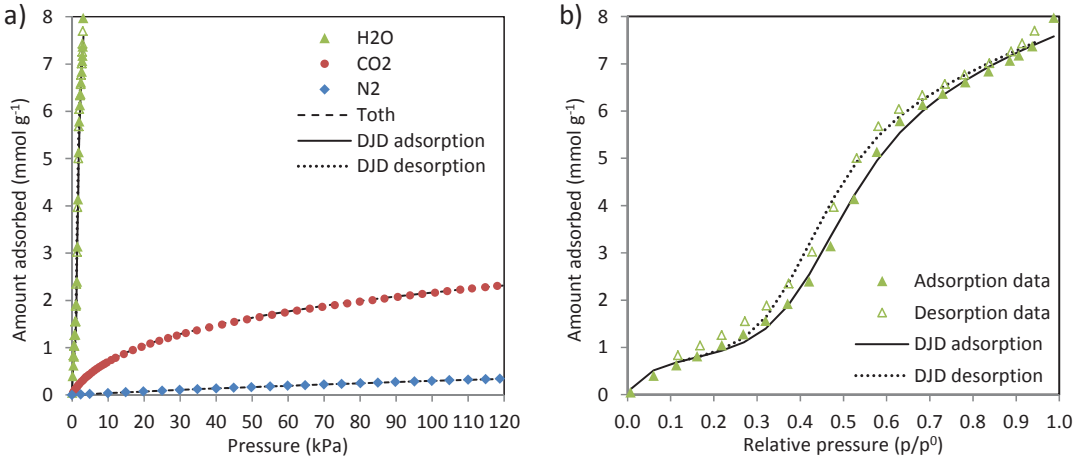

Fig. 2. (a) Comparison of the adsorption isotherms of CO_2, N_2 and H_2O at 25 °C; (b) water vapor adsorption and desorption isotherm at 25 °C; (symbols represent experimental data and lines the prediction of the DJD model)

The equilibrium of adsorption of pure CO_2 and N_2 can be described by the relatively simple Toth model [2]. However, the equilibrium of adsorption of water vapor cannot be properly described by this equation. Over the years, specific adsorption models have been developed for the adsorption of water vapor on carbon materials that adequately describe the Type V topology. To the authors knowledge, only one model has been proposed that describes the adsorption and desorption of water vapor on microporous carbons in the entire relative pressure range: the model proposed by Do, Junpirom and Do (DJD) (Equations 1 and 2, respectively) [11]. This model considers that water adsorption initiates on the surface functional groups located at the graphene edges, and proceeds by H-bonding of new water molecules that form growing clusters until they attain a sufficient size to enter the micropores. An extension of this model was later proposed by Horikawa and Do to account for the adsorption of water vapor in the mesopores [12].

$$C_{DJD,adsorption} = S_0 \frac{k_f \sum_{n=1}^{m} n x^n}{1 + K_f \sum_{n=1}^{m} x^n} + C_{\mu s} \frac{k_\mu \sum_{n=\alpha_\mu+1}^{m} x^n}{k_\mu \sum_{n=\alpha_\mu+1}^{m} x^n + \sum_{n=\alpha_\mu+1}^{m} x^{n-\alpha_\mu}} \quad (1)$$

$$C_{DJD,desorption} = S_0 \frac{k_f \sum_{n=1}^{m} n x^n}{1 + k_f \sum_{n=1}^{m} x^n} + C_{\mu s} \frac{k_\mu \left(1 + K_{R\mu}\right) \sum_{n=\alpha_\mu+1}^{m} x^n}{k_\mu \left(1 + K_{R\mu}\right) \sum_{n=\alpha_\mu+1}^{m} x^n + \sum_{n=\alpha_\mu+1}^{m} x^{n-\alpha_\mu}} \quad (2)$$

$$Objective\ function = \sum_{i=1}^{N} \left(C_{exp} - C_{calc}\right)_i^2 \quad (3)$$

The DJD model parameters S_0, k_f, α_μ, $C_{\mu s}$, and k_μ were fitted to minimize the sum of square residuals (Equation 3) between the adsorption isotherm at 25 °C and the values calculated using Equation 1. The value of m was set to: $m=\alpha_\mu+1$ [12]. The relaxation equilibrium constant for water desorption from the micropores, $k_{R\mu}$, was fitted to minimize the sum of square residuals between the desorption isotherm and the values calculated using Equation 2. The DJD parameters are shown in Table 3, and the goodness of fit can be observed in Figure 2b. The DJD adsorption model represents adequately the experimental adsorption isotherm up to relative pressures of 0.95, and the DJD desorption model gives an approximated description of the hysteresis loop.

Table 3. Optimal parameters of the DJD model

Temperature (°C)	S_0 (mmol g^{-1})	k_f	α_μ	$C_{\mu s}$ (mmol g^{-1})	k_μ	$k_{R\mu}$
25	0.81	22.91	6	4.46	69.21	0.89

The value obtained for S_0 represents 39 % of the total oxygen content of the carbon; this was to be expected, as not all the oxygen is necessarily available for the adsorption of H_2O. The size of the water clusters in the micropores (α_μ) depends mainly on the pore size of the carbon, although it is also affected by the surface chemistry that can contribute to stabilize smaller clusters [11]. The value obtained for α_μ is relatively low, which is attributed to the narrow size of the micropores of the biochar evaluated. In fact, this value is lower than that obtained for an activated carbon developed from the same precursor by activation with CO_2 which presents a slightly higher oxygen content but wider micropore width [4]. $C_{\mu s}$ represents 30% of the physical upper limit, which was calculated assuming that all the micropore volume is completely full of liquid water at the adsorption temperature. This packing fraction in the micropores is also lower than that obtained for an activated carbon developed from the same precursor by activation with CO_2, due to the narrower pore size of the biochar activated with air [4].

3.2. Dynamic experiments: influence of water vapor on CO_2 capture

Figure 3a shows the molar flow rate of CO_2 and N_2 in the effluent during the dry and wet breakthrough experiments (runs 1-4). At $t = 0$ the synthetic flue gas mixture is fed to the adsorber, which is initially regenerated and filled with helium. N_2 breaks through the bed in first place: the molar flow rate of N_2 in the effluent increases rapidly, meeting that of the feed in approximately 4 min. On the other hand, the molar flow rate of CO_2 in the effluent goes through a minimum at around 3 min, and then starts to increase meeting the feed flow rate in about 11 min. During this time, the effluent is enriched in N_2 and depleted from CO_2 due to the preferential adsorption of CO_2 over N_2. Note that the CO_2 breakthrough curves obtained using the dry gas (runs 1 and 3) and the moist gas (runs 2 and 4) overlap each other. These results seem to indicate that the presence of water vapor does not hinder the adsorption of CO_2 on the evaluated biochar.

The molar flow rate of water vapor in the effluent during the breakthrough curves (runs 1-4) is shown in Figure 3b. When the moist gas is fed to the adsorber at $t = 0$ (runs 2 and 4), the water vapor flow rate in the effluent starts to decrease due to the adsorption of water vapor by the biochar. This decay continues for approximately 95 min, and then starts to increase again for another 300 min, stabilizing thereafter. However, the flow rate of water vapor in the effluent does not met that of the feed at *t=0*. The relative humidity of the effluent stabilizes in a value of 53 %, which is below the initial value of the feed (65 %). The evolution of the water flow rate in the effluent during the first 15 min of runs 1-4 is shown in greater detail in the upper part of Figure 4b to facilitate comparison with the breakthrough curves of N_2 and CO_2 (Figure 3a). Note that the adsorbent is rapidly saturated by N_2 and CO_2 but it is very slowly saturated by H_2O. Run 2 was stopped after the water breakthrough, but run 4 was continued for nearly 8 h (see the good agreement between the breakthrough of water vapor in runs 2 and 4 in Figure 3b). The water breakthrough curve is initially steep, but after 1 h the slope decays to increase again by the end of the experiment. The shape of the breakthrough curves is intrinsically related to the equilibrium of adsorption [13] and the adsorption rate of water vapor on carbon adsorbents displays a widely varying time scale [14, 15]. In the present case, three distinct regions can be identified in the breakthrough curve: the first region (steep breakthrough) takes place when the relative humidity of the effluent is below 20%; in the adsorption isotherm, this corresponds to the adsorption of water molecules around the functional groups. The second region, between 20 and 40% RH, presents a lower slope, and is related to the cooperative adsorption of water molecules (growth of water clusters around the functional sites). The third region, which is again steeper, takes place for relative humidities of the effluent between 40 and 60 %, and corresponds to the filling of the micropores in the equilibrium adsorption isotherm (Figure 2b).

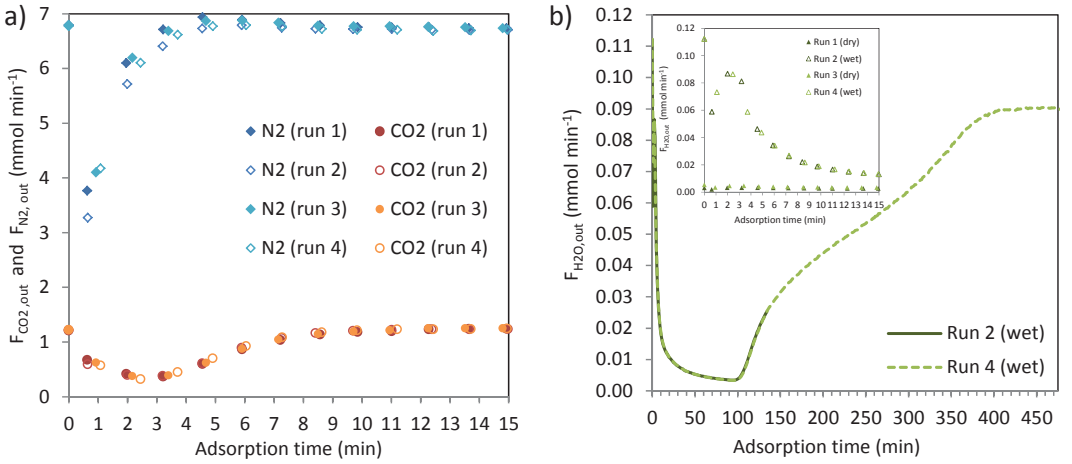

Fig. 3. Component molar flow rates in the effluent during runs 1-4: (a) CO_2 and N_2 (b) H_2O.

The amount of especies *i* adsorbed at a given time (*t*) can be estimated by making a partial mass balance to the adsorber and discounting the gas retained in the void volume (Equation 4). The amount of CO_2 adsorbed during the first 11 min of the breakthrough experiments carried out in the presence and absence of water vapor (runs 1-4) is similar to the value predicted by the pure component Toth model: 1.1 mmol g^{-1}. This confirms that the presence of water vapor in the gas mixture does not diminish the CO_2 adsorption capacity of the biochar in the short time scale due to the delayed adsorption of water vapor. The amount of water vapor adsorbed in the same period of time during the wet runs (2 and 4) is only 0.2 mmol g^{-1}, which represents about 3-4 % of its pure equilibrium adsorption capacity.

$$C_i = \frac{\int_{t=0}^{t}(F_{i,in}-F_{i,out})dt-\frac{P(y_{i,t}-y_{i,t=0})}{RT}(\varepsilon V_b+V_d)}{w} \quad (4)$$

Only the mass flow rate of the effluent and its composition were monitored continuously during the experiment. To calculate the amount adsorbed at short time scales, it was assumed that $F_{i,in} = F_{i,t=0}$. However, when the time of integration is large, small absolute changes in the flow rate of each species fed to the adsorber can cause a relatively large accumulated error in the integration term. For this reason, the amount of water vapor adsorbed during run 4 was estimated from the desorption curve (Figure 4b) making use of equation 4 ($F_{H2O,in}=0$). The total amount of H_2O desorbed during the regeneration of the adsorbent with helium flow at 150 °C was 5.6 mmol g^{-1}; this amount falls within the equilibrium capacity of pure water vapor at 25 °C in the relative humidity range between 53 and 65 %. The amount of CO_2 desorbed during the regeneration of run 4 was 0.6 mmol g^{-1} which means that part of the CO_2 initially adsorbed was progressively displaced by the preferential adsorption of H_2O. However, it is important to highlight that the adsorption capacity of CO_2 in the short time scale, which is relevant for industrial adsorption processes, is not affected by the presence of water vapor. Another important advantage from the point of view of the future cyclic adsorption performance is that the adsorbent recovers full adsorption capacity after regeneration. The time required to fully regenerate the adsorbent was similar to the length of the adsorption experiment. Using short adsorption times the amount of water adsorbed will be low and fast to desorb. CO_2 is more readily desorbed than H_2O: the conditions of the regeneration step should be carefully selected to maximize CO_2 purity with the minimal energy consumption.

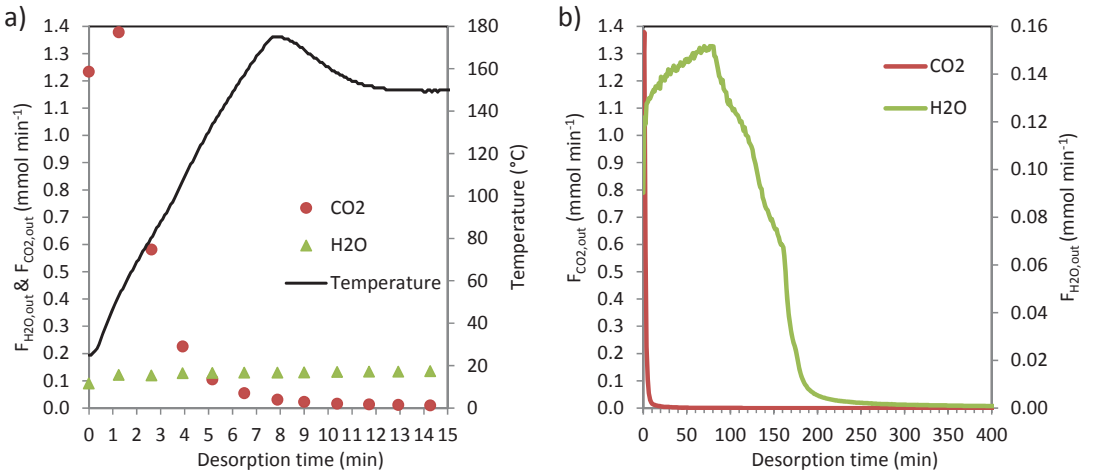

Fig. 4. CO_2 and H_2O molar flow rates during the regeneration of run 4: (a) detail of the first 15 min and (b) 400 min.

4. Conclusions

In this work, the effect of water vapor on the adsorption of CO_2 using a microporous biochar obtained by direct activation of olive stones with air is assessed. The equilibrium of adsorption of water vapor in the temperature range between 12.5 and 85 °C was studied. The evaluated biochar presents a moderate adsorption capacity of water vapor, and the isotherms present a type V topology with low uptakes at low relative pressures and a narrow hysteresis loop. These characteristics are of interest as they will facilitate the desorption of water vapor during the regeneration step in a cyclic process. It was observed that the temperature affects the equilibrium of adsorption of water vapor mainly by the shift in the saturation pressure. The equilibrium of adsorption of water vapor on the evaluated biochar can be described by specific adsorption models developed for carbon materials. These model equations can be implemented in simulation tools to account for the presence of water vapor in flue gas during the design of the separation process.

Multicomponent experiments carried out in a fixed-bed adsorption unit in the presence and absence of water vapor demonstrated that the biochar adsorbs preferentially CO_2 over N_2 in conditions representative of postcombustion applications. Although H_2O is also adsorbed by the biochar, no significant reduction in the CO_2 adsorption capacity was observed in the short time scale in the presence of water vapor. This is attributed to the delayed adsorption of H_2O. If adsorption is continued for a sufficiently long time, the adsorption of H_2O can displace part of the previously adsorbed CO_2. However, cyclic processes use short adsorption times, where the influence of water vapor is negligible. Moreover, the adsorbent recovered full adsorption capacity after regeneration, which is mandatory for an efficient cyclic adsorption/desorption performance. These findings, together with the availability and low-cost inherent to the biochar, confirm the interest of this material for postcombustion CO_2 capture applications.

Acknowledgements

Work carried out with financial support from the Spanish MINECO (Project ENE2011-23467), co-financed by the European Regional Development Fund (ERDF). M.G.P. acknowledges funding from the CSIC (JAE-Doc program) and A.S.G. acknowledges a contract from the Spanish MINECO (FPI program), both programs are co-financed by the European Social Fund.

References

[1] Wang L, Yang Y, Shen W, Kong X, Li P, Yu J, Rodrigues AE. Experimental evaluation of adsorption technology for CO_2 capture from flue gas in an existing coal-fired power plant. *Chemical Engineering Science* 2013; **101**(0): 615-9.

[2] Plaza MG, González AS, Pis JJ, Rubiera F, Pevida C. Production of microporous biochars by single-step oxidation: Effect of activation conditions on CO_2 capture. *Appl Energ* 2014; **114**(0): 551-62.

[3] IPCC, *IPCC special report on carbon dioxide capture and storage*. IPCC. Cambridge, United Kingdom and New York, NY, USA: 2005.

[4] Plaza MG, González AS, Pevida C, Rubiera F. Influence of water vapor on CO_2 adsorption using a biomass-based carbon. *Ind Eng Chem Res* Article ASAP; DOI: 10.1021/ie500342q.

[5] Tsunoda R. Adsorption of water vapor on active carbons: Estimation of pore width. *J Colloid Interface Sci* 1990; **137**(2): 563-70.

[6] Perry RH, Green DW. *Perry's Chemical Engineers' Handbook*. 7th ed.: McGraw-Hill; 1997

[7] Cortés FB, Chejne F, Carrasco-Marín F, Moreno-Castilla C, Pérez-Cadenas AF. Water adsorption on zeolite 13X: comparison of the two methods based on mass spectrometry and thermogravimetry. *Adsorption* 2010; **16**(3): 141-6.

[8] Xu D, Xiao P, Zhang J, Li G, Xiao G, Webley PA, Zhai Y. Effects of water vapour on CO_2 capture with vacuum swing adsorption using activated carbon. *Chem Eng J* 2013; **230**(0): 64-72.

[9] Rudisill EN, Hacskaylo JJ, LeVan MD. Coadsorption of hydrocarbons and water on BPL activated carbon. *Ind Eng Chem Res* 1992; **31**(4): 1122-30.

[10] González AS, Plaza MG, Rubiera F, Pevida C. Sustainable biomass-based carbon adsorbents for post-combustion CO_2 capture. *Chem Eng J* 2013; **230**(0): 456-65.

[11] Do DD, Junpirom S, Do HD. A new adsorption–desorption model for water adsorption in activated carbon. *Carbon* 2009; **47**(6): 1466-73.

[12] Horikawa T, Sekida T, Hayashi Ji, Katoh M, Do DD. A new adsorption–desorption model for water adsorption in porous carbons. *Carbon* 2011; **49**(2): 416-24.

[13] Ruthven DM. *Principles of adsorption and adsorption processes*. New York: John Wiley and Sons; 1984

[14] Cossarutto L, Zimny T, Kaczmarczyk J, Siemieniewska T, Bimer J, Weber JV. Transport and sorption of water vapour in activated carbons. *Carbon* 2001; **39**(15): 2339-46.

[15] Rutherford SW. Modeling water adsorption in carbon micropores: study of water in carbon molecular sieves. *Langmuir* 2006; **22**(2): 702-8.